JASA ARTICLE

Characterizing the acoustic response of *Thalassia testudinum* leaves using resonator measurements and finite element modeling

Nicholas A. Torres,[1] Megan S. Ballard,[2,a)] Kevin S. Lee,[2] Preston S. Wilson,[1,b)] Christina J. Naify,[2] and Aytahn Ben-avi[2]

[1]*Walker Department of Mechanical Engineering, The University of Texas at Austin, Austin, Texas 78712-0292, USA*

[2]*Applied Research Laboratories, The University of Texas at Austin, Austin, Texas 78713-8029, USA*

ABSTRACT:

Seagrasses play an important role in coastal ecosystems and serve as important marine carbon stores. Acoustic monitoring techniques exploit the sensitivity of underwater sound to bubbles, which are produced as a byproduct of photosynthesis and present within the seagrass tissue. To make accurate assessments of seagrass biomass and productivity, a model is needed to describe acoustic propagation through the seagrass meadow that includes the effects of gas contained within the seagrass leaves. For this purpose, a new seagrass leaf model is described for *Thalassia testudinum* that consists of a comparatively rigid epidermis that composes the outer shell of the leaf and comparatively compliant aerenchyma that surrounds the gas channels on the interior of the leaf. With the bulk modulus and density of the seagrass tissue determined by previous work, this study focused on characterizing the shear moduli of the epidermis and aerenchyma. These properties were determined through a combination of dynamic mechanical analysis and acoustic resonator measurements coupled with microscopic imagery and finite element modeling. The shear moduli varied as a function of length along the leaves with values of 100 and 1.8 MPa at the basal end and 900 and 3.7 MPa at the apical end for the epidermis and aerenchyma, respectively.

 https://doi.org/10.1121/10.0017000

(Received 17 August 2022; revised 22 December 2022; accepted 6 January 2023; published online 27 January 2023)

[Editor: Grant B. Deane] Pages: 678–688

I. INTRODUCTION

Seagrasses play an important role in coastal ecosystems through stabilizing the sediment, sequestering carbon, cycling nutrients, and providing a habitat for marine life. They also act as ecosystem health indicators in that changes in seagrass abundance or distribution signify changes in environmental conditions (Orth *et al.*, 2006). Rapid degradation of seagrass beds threatens the health of coastal ecosystems worldwide (Waycott *et al.*, 2009). Both natural and anthropogenic disturbances, which result in the devegetation of areas within a seagrass meadow, can be found in shallow-water coastal regions, and accurately quantifying and characterizing the deterioration of these ecosystems is of great interest. To probe these ecosystems, ecologists have traditionally relied on satellite imagery and aerial photography to create maps of the seagrass meadows. However, the efficacy of these approaches depends on a variety of external factors, including meteorological conditions and water turbidity. In particular, these optical methods are subject to light attenuation due to water depth, sediment load, and microalgae in the water column, as well as wave action due to meteorological conditions and wakes from watercraft. These factors limit the effectiveness of using optical methods to map the sea floor. As a result, it is often not possible to accurately quantify the health of seagrass meadows beyond a simple visual inspection.

Sonar-based techniques have been proposed as an alternative to traditional optical methods (Gumusay *et al.*, 2019). These sonars emit high-frequency acoustic pulses, which are then reflected back by the seabed and sensed by a receiving transducer. The images created by the sonar depend on the intensity and delay of the echoes [see Fig. 1(a)]. Sonar images have been applied for coastal mapping of submerged aquatic vegetation using side-scan sonar (Bennett *et al.*, 2020; Greene *et al.*, 2018; Klemens, 2017; Pasqualini *et al.*, 1999; Pergent *et al.*, 2017; Stocks *et al.*, 2019; van Rein *et al.*, 2011) as well as single-beam and multibeam echosounders (Hamana and Komatsu, 2016; Held and Schneider von Deimling, 2019; Kruss *et al.*, 2017; van Rein *et al.*, 2011). The standard approach is to segment the sonar images into regions of healthy seagrass and disturbed regions. Analysis of side-scan imagery has traditionally relied on trained analysts to produce maps of seagrass cover (Bennett *et al.*, 2020). Automatic classification methods based on gray-level co-occurrence matrices, filtering, thresholding, statistical clustering, and principle component analysis as well as machine learning techniques, including support vector machines, random forest, and decision trees,

a)Electronic mail: meganb@arlut.utexas.edu

b)Also at: Applied Research Laboratories, The University of Texas at Austin, Austin, TX 78713-8029, USA.

https://doi.org/10.1121/10.0017000

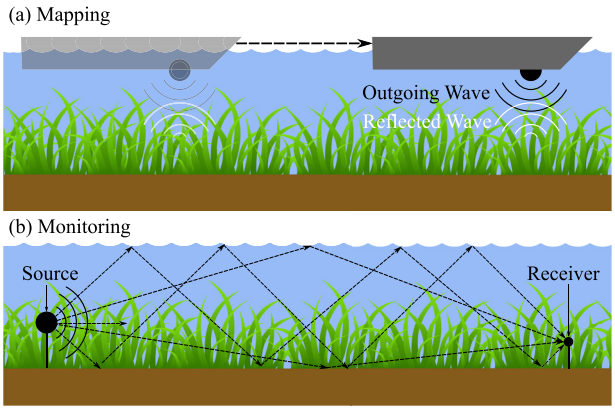

FIG. 1. (Color online) Schematic diagrams showing (a) acoustic mapping of a seagrass meadow using a sonar on a moving platform to make a measurement at single point in time and (b) acoustic monitoring using a stationary system to make measurements over a period of time from a single point to space.

have been applied to side-scan imagery of seagrass meadows (Gumusay *et al.*, 2019; Rahnemoonfar and Dobbs, 2019).

Acoustic remote sensing techniques for monitoring seagrass meadows were first proposed by Hermand *et al.* (1998) and further investigated by Ballard *et al.* (2020), Chang *et al.* (2019), Felisberto *et al.* (2015), Hermand (2004), Hermand *et al.* (2000), Lee *et al.* (2023), and Lee *et al.* (2019). These approaches are based on the propagation of sound through the seagrass meadow to estimate seagrass health parameters such as biomass or photosynthetic rates [see Fig. 1(b)]. These techniques exploit the sensitivity of underwater sound to bubbles, which are produced as a byproduct of photosynthesis and are also present within the seagrass tissue. To make accurate assessments of seagrass biomass and productivity from acoustic measurements, a model is needed to describe acoustic propagation through the seagrass meadow that includes the effects of gas contained within the seagrass leaves. Previous efforts to estimate the volume fraction of gas (Ballard *et al.*, 2020; Hermand *et al.*, 2000) relied on simplified models for sound propagation through bubbly liquids (Commander and Prosperetti, 1989; Mallock, 1910; Wood, 1946). Although suitable for the initial work, the physical model applied in these studies was an oversimplification of the actual environment; hence, the resulting parameter estimates and uncertainties may be strongly biased (Ballard *et al.*, 2020).

In parallel with the field work described above, an understanding of the physical parameters of seagrass leaves important for characterizing its acoustical effects was built up through a series of laboratory measurements. Resonator experiments were carried out to measure the low-frequency effective sound speed of seagrass in a column of seawater. These experiments have led to increasingly more complex models for seagrass leaves to explain the measured acoustic response. The simplest model assumed the seagrass tissue had a negligible effect on the acoustic response, and the tissue properties were set as equivalent to the surrounding seawater (Wilson and Dunton, 2009). The Mallock–Wood equation (Mallock, 1910; Wood, 1946) was applied to estimate the volume fraction of gas in the resonator. Failure of this model to accurately estimate the volume of gas assessed from microscopic images of cross sections of the seagrass leaves led to the development of a more complex fluid model, which considered the compressibility of the seagrass tissue as opposed to solely the gas bodies (Wilson *et al.*, 2010). Both a three-phase model and nested scheme with the Mallock–Wood equation were applied in an attempt to determine the compressibility of the seagrass tissue. Ultimately, this model yielded only non-physical results, which led to the conclusion that a fluid effective-medium model was insufficient; the elastic properties and the physical structure of seagrass needed to be considered.

The approaches described above neglected the effects of elastic properties of seagrass tissue as well as the shape of the aspherical gas bodies constrained within the plant and also neglected any variability along the length of the leaf. To rectify this, a finite element method (FEM) model of the seagrass leaf was developed based on existing resonator measurements and microscopic imagery of *Thalassia testudinum* from Wilson and Dunton (2009). The results of this study inferred a shear modulus for the seagrass tissue that provided excellent agreement with the measured effective sound speed (Torres *et al.*, 2020). However, this acoustically determined shear modulus disagreed with an independent measurement of the shear modulus determined with a low-frequency torsional vibration technique (Venegas *et al.*, 2020). The disparity in the shear moduli estimated from these techniques motivated the development of a new seagrass leaf model that is the focus of the current paper. The new leaf model was informed by microscopic imagery of seagrass leaves that shows clear evidence of a stiffer epidermis layer that encapsulates a more compliant aerenchyma that contains the lacunae. To evaluate the new leaf model, a new set of resonator measurements was collected with supporting microscopic imagery. The images were analyzed and used with a FEM model to estimate the shear moduli of the epidermis and aerenchyma of the seagrass leaf.

This study also takes into account variability along the length of the seagrass leaves. A previous study focused on two Mediterranean species found that the basal ends of the leaves were characterized by greater void fractions and channels with larger cross-sectional areas (Johnson, 2019). Ultrasonic measurements of sound speed and attenuation were also acquired along the length of the leaves. *Posidonia oceanica* had decreased sound speed and increased attenuation near the basal ends, whereas the acoustic properties of *Cymodocea nodosa* were nearly constant along the length of the leaves.

This paper concentrates on *Thalassia testudinum*, one of three dominant species of the Tropical Atlantic bioregion (Short *et al.*, 2007). *T. testudinum* has been the most pervasive species in recent field studies in the Texas coastal areas, including the Lower Laguna Madre (Ballard *et al.*, 2020; Lee *et al.*, 2019) and Corpus Christi Bay (Ballard *et al.*, 2022; Lee *et al.*, 2017). *T. testudinum* forms meadows in

shallow sandy or muddy sediments. It is a perennial grass growing from a long, jointed rhizome, which is buried in the substrate 5–10 cm deep. Wide, flat, ribbon-like blades with rounded tips grow from the rhizomes to lengths of up to 30 cm with widths of 2 cm. Both the above- and below-ground biomass exhibit seasonal growth patterns correlated with underwater irradiance, day length, and temperature (Kaldy and Dunton, 2000; Lee and Dunton, 1996).

This paper has the following organization. Section II describes the methods, including the acoustic resonator measurements, torsional measurements, analysis of microscopic imagery, and FEM modeling. The results are presented in Sec. III, and the discussion is contained in Sec. IV. Conclusions and future work are presented in Sec. V.

II. METHODS

The seagrass leaves examined in this study were collected in the East Flats area of Corpus Christi Bay near the Texas Gulf of Mexico coast during the summer season. Whole plants were collected in 15-cm-diameter cores with the root system and sediment intact. The cores were transported to the University of Texas at Austin for laboratory measurements. The seagrass plants were stored in a saltwater aquarium and kept alive and healthy with adequate light and aeration for several weeks. Leaves were removed from the plants for the experiments and analysis described below.

A. Resonator measurements

As described in the Introduction, acoustic resonators have been used to measure the frequency-dependent sound speed of a mixture of seagrass leaves and seawater. This approach uses observations of the system's fundamental frequencies to determine the effective sound speed of the material within the resonator. For a uniform rigid-walled waveguide of length h with pressure release end conditions (Dolder and Wilson, 2017; Lee *et al.*, 2011; Wilson and Dunton, 2009; Wilson and Roy, 2008), the eigenfunction $\Psi_n(z)$ for the nth mode is given by

$$\Psi_n(z) = a_n \sin\left(\frac{\pi z}{h}\right), \tag{1}$$

where z is the position along the resonator tube. These modes represent plane waves traveling in the $\pm z$ direction that form standing waves in the resonator tube. The modal eigenfrequency f_n for the nth mode is given by

$$f_n = \frac{c_n n}{2h}, \tag{2}$$

where c_n is the modal phase speed, which represents the frequency-dependent effective sound speed of the material inside the resonator. Below the resonance frequency of the bubbles encapsulated within the seagrass tissue, the sound speed of the mixture of seagrass leaves and seawater is lower than that of seawater only. Within this low-frequency regime, the effective sound speed is nearly constant over frequency. At resonance, the effective sound speed of the mixture has a minimum value, and attenuation is at a maximum (Church, 1995; Commander and Prosperetti, 1989).

In this work, the resonator experiments used a 611-mm-tall glass cylindrical resonator tube with inner and outer diameters of 51.5 and 70.0 mm, respectively. The bottom end of the resonator tube was sealed with a thin rubber membrane and was placed on an 11-cm-thick stack of Styrofoam blocks to approximate a pressure release boundary condition. The water-filled tube was open on the top to establish a very nearly pressure release boundary condition at the air-water interface. A 38-mm-diameter circular piston was inserted into the top of the resonator tube and driven by an electromagnetic shaker to excite the acoustic response of the system. The excitation signal was a linear chirp in the 200 Hz to 5 kHz frequency band. A hydrophone was used to measure the acoustic field inside the tube at a distance of approximately 40 mm from the open end. A laptop computer coupled with a portable data acquisition system and its associated software was used to generate the source signal, which was directed to a power amplifier and then to the shaker. The hydrophone signal was conditioned by a preamplifier, digitized, and recorded on the laptop. Figure 2 shows a schematic of the experimental apparatus.

Following Lafleur and Shields (1995), the Del Grosso (1971) model was used to correct for the elastic waveguide effects resulting from the glass walls of the resonator tube. The model was applied to the resonator measurements in two steps. First, the model was calibrated using a reference measurement of a seawater-filled tube to determine the elastic modulus of the glass (Torres, 2022; Wilson *et al.*, 2007). Tabulated values were used for the Poisson's ratio, Young's modulus, and density of glass. Then the calibrated model

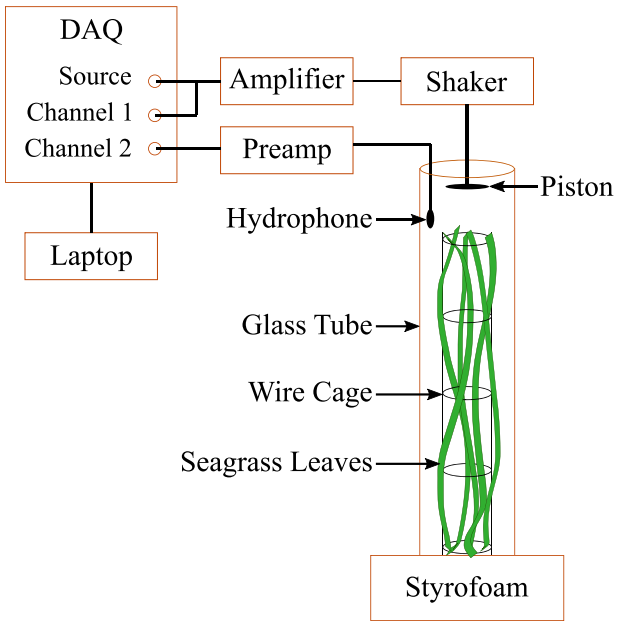

FIG. 2. (Color online) Schematic diagram showing the acoustic resonator and data acquisition instrumentation. The helical orientation of the seagrass in shown in the resonator tube.

https://doi.org/10.1121/10.0017000

was applied to determine the effective sound speed when the seagrass leaves were added to the seawater. This approach used an iterative process by which the effective sound speed of the seawater-seagrass mixture was perturbed until the modal phase speeds predicted by the model were brought into agreement with the measurements.

A wire cage was used to secure the seagrass leaves in place during the resonator measurements. The cage was composed of 22 gauge (0.6426 mm diameter) tinned-copper bus bar wire consisting of four vertical wires, with seven horizontal circular wires. The intersections of the vertical and horizontal wires served as attachment points for the seagrass leaves. The seagrass leaves were attached to the wire cage by threading nylon monofilament line through the leaves and tying them in place to hold them in a specified orientation. The addition of the wire cage to the resonator tube caused a minimal shift of the resonance frequencies ($<0.5\%$), and the effect of the monofilament line was negligible based on the results of preliminary measurements. Throughout the attachment process, the leaves were periodically submerged in seawater to keep them from drying out.

For the experiments presented in this paper, the resonator tube was filled with seawater. Degassed seawater was used to fill the bottom portion of the resonator tube to minimize the effect of bubbles that could be trapped between the thin rubber bottom and the glass tube. The rest of the tube was then filled with non-degassed seawater using tubing as a siphon to minimize the introduction of bubbles to the system. This differs from other resonator measurements that typically use degassed water (Dolder and Wilson, 2017) so that any bubbles introduced into the resonator can be absorbed into the under-saturated water. However, when seagrass was placed in degassed water, the gas from the lacunae diffused through the seagrass tissue into the surrounding seawater (see the Appendix). Instead, after attaching the seagrass leaves to the cage, the assembly was submerged in degassed water before placement in the resonator tube. The coating of degassed water was a preventive measure against bubble formation. The resonator experiments were performed in low-light conditions to prevent the seagrass leaves from photosynthesizing and producing bubbles in the surrounding seawater. Hence, the change in the effective sound speed in the resonator measurements was attributed to the presence of the seagrass and the gas contained within the aerenchyma.

B. Microscopic imagery

Microscopic imagery of the seagrass leaves was obtained to provide a measurement of the seagrass leaves' characteristics, including the void fraction of gas present in the leaves, the quantity and thickness of the two types of seagrass tissue (epidermis and aerenchyma), and the size and shape of the gas channels and their variation along the length of the leaf.

The microscopic imagery of the seagrass was obtained by cutting a thin slice from a seagrass leaf perpendicular to the length direction. The slice was placed on a microscope slide with seawater and a coverslip to keep it from drying out and to hold its orientation flat. The slide was placed on the optical microscope, and imagery was collected. Images of cross-sections were used from different locations along the length of each leaf to characterize the variation of the internal structure between the basal and apical ends. The total volume of gas present in the seagrass leaves was determined by multiplying the area of the channels by the length of the associated leaf section. The total volume of each leaf was determined in a similar manner using the total cross section area. Finally, the void fraction was calculated as the volume ratio of gas to total leaf volume.

C. Torsional measurements

The shear modulus of seagrass leaf sections was characterized using a dynamic mechanical analyzer (DMA). The DMA was configured to apply a sinusoidal torsional force and measure the strain in the leaf under ambient temperature and pressure in the laboratory. Measurements were acquired over a frequency range 0.1–20 Hz and under a tension of 0.1 N. The DMA software used the outer dimensions of the specimen to compute the shear modulus of the material under the assumption its properties are homogeneous. Hence, the shear modulus of the seagrass leaf reported by the DMA measurements is an effective shear modulus and represents that of the composite leaf structure inclusive of both the epidermis and aerenchyma.

D. FEM model

This work uses FEM simulations in COMSOL to model the resonator experiment described above. Previous work determined that three-dimensional (3D), two-dimensional (2D) axisymmetric, and 2D rectangular geometries yielded similar results. Each domain produced an effective sound speed within 1% of the other domains when they were supplied with identical void fractions (Torres *et al.*, 2020). Based on these results, this work uses a 2D rectangular domain as it is the most computationally efficient. In this domain, the cylindrical resonator is modeled as a 2D rectangle with rigid boundaries on the long sides (analogous to the diameter of the resonator) and pressure release boundaries on the short sides (analogous to the top and bottom of the resonator). The seagrass leaves are represented as leaf cross sections that include the epidermis, aerenchyma, and lacunae. Variability along the length of the seagrass leaf is accounted for by including leaf cross sections from different parts of the leaf.

The system response was calculated for a monopole source using a frequency sweep over the same range of frequencies as the measured data. As with the measurements, the resonance frequencies were estimated from the system response. Because the simulations used idealized boundary conditions, the effective sound speed was determined directly from Eq. (2), without the need for the Del Grosso (1971) model.

In the simulations, the height of the resonator tube was set to match that of the measurements, and the width of the 2D domain was adjusted so that the gas volume fraction in the FEM model matched that of the resonator experiments. The seagrass leaves were generated from the microscopic imagery, such that each cross-sectional image represents a 2D leaf. Unless otherwise noted, each experiment used cross sections from the basal, middle, and apical leaf sections to account for variability along the leaf. The leaves were constructed in the FEM simulations to consist of three components, each having uniform properties: epidermis, aerenchyma, and gas channels. The simulations were designed to match the volume fraction of seagrass tissue and volume fraction of gas from the measurements with equivalent area fractions in the model.

III. RESULTS

A. Resonator measurements

1. Leaf orientation

A set of resonator measurements was collected to investigate the dependence of the low-frequency response of seagrass leaves on the orientation of the leaves inside the resonator. Previous work, which considered a single set of resonator measurements of the Mediterranean species *C. nodosa*, suggested that leaf orientation may be important (Johnson, 2019). However, this result is not consistent with FEM simulations of *T. testudinum*, which showed no discernible change in acoustic response for 3D vertically orientated simulations compared to 2D axisymmetric and 2D rectangular simulations (Torres *et al.*, 2020).

This experiment used the same set of ten seagrass leaves attached to the bus bar wire frame in four different orientations. The volume fraction of seagrass in the resonator was 5.37×10^{-3} (includes gas), and the volume fraction of gas (contained within the aerenchyma) in the resonator was 7.16×10^{-4}. The four orientations were (1) vertical with the basal end at the bottom of the resonator, (2) vertical with the apical end at the bottom of the resonator, (3) vertical with half the leaves having the basal end at the bottom and half with the apical end at the bottom, and (4) approximately horizontal with the leaves curved around the wire frame. A fifth set of measurements was collected with the leaves in the original orientation (basal end at the bottom) to assess measurement drift over time due to gas diffusion and/or damage to the leaves from repeated connections to the wire frame. Five replicate data collections were performed for each orientation, where the placement of the leaves was adjusted by rotating the cage. The mean effective sound speed and its standard deviation were calculated for each of the resonance peaks. The results are plotted as the ratio of effective sound speed to seawater sound speed in Fig. 3. In the figure, the effective sound speed determined from the first resonance was omitted because it was biased by a structural mode of the glass resonator tube. Following other resonator studies (Lenhart *et al.*, 2016), the structural mode was identified using a laser Doppler vibrometer (LDV) to measure vibrations in the glass tube that could indicate interference with the acoustic measurements (Torres, 2022).

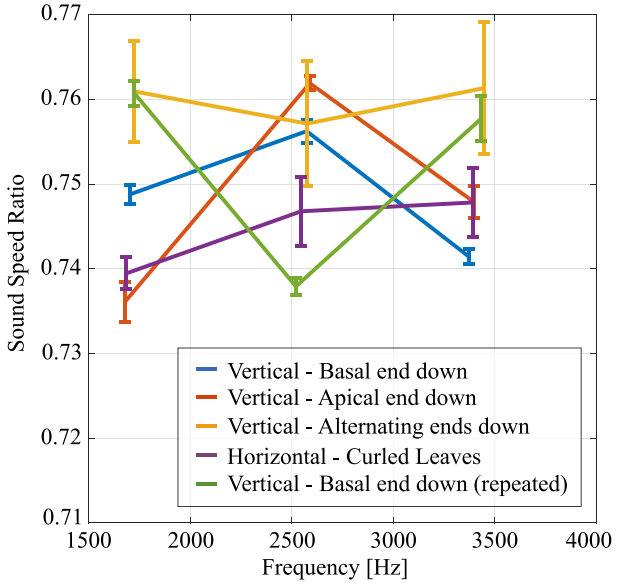

FIG. 3. (Color online) Sound speed ratios calculated from resonator experiments using different leaf orientations. Error bars represent the standard deviation of five sets of replicate measurements.

The sound speed ratio for all five sets of measurements across the entire frequency band is bounded between approximately 0.74 and 0.76. The intra-measurement variability is greater than the difference between the measurements from the various leaf orientations. These results suggest that the low-frequency response of *T. testudinum* does not depend on seagrass leaf orientation.

2. Variability along leaf length

Variability of the effective sound speed along the length of seagrass leaves was quantified by a set of resonator measurements that considered the leaf sections: basal, middle, and apical. The sections were created by cutting each seagrass leaf into three equally long sections. To collect the measurements, the leaves from each section were attached to the wire cage, and five replicate measurements were acquired with rotations of the cage. The experiment was repeated for leaves from the basal section, middle section, and apical section. The volume fractions of seagrass leaves and gas within the resonator are summarized in Table I. The effective sound speeds calculated from the resonator measurements are shown in Fig. 4. As before, the first mode is omitted due to interference with a structural mode of the

TABLE I. The volume fraction of seagrass leaves in the resonator and the volume fraction of gas (contained within the aerenchyma) in the resonator.

Section	Leaves	Gas
Apical	1.35×10^{3}	1.17×10^{4}
Middle	1.16×10^{3}	1.62×10^{4}
Basal	2.43×10^{3}	4.36×10^{4}

https://doi.org/10.1121/10.0017000

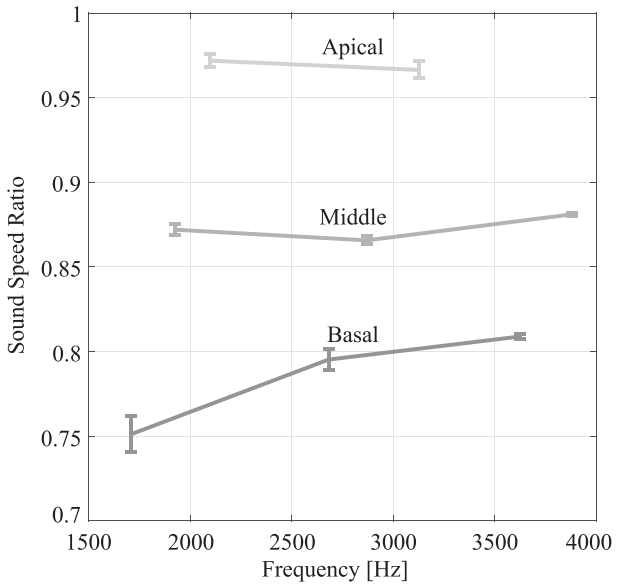

FIG. 4. Sound speed ratios calculated from resonator experiments on the basal, middle, and apical leaf sections. Error bars represent the standard deviation of five sets of replicate measurements.

resonator. The fourth mode from the apical measurements was affected by the resonance of the piston and was also omitted from the figure. The separation in the effective sound speed measurements between the basal, middle, and apical sections is evidence that the acoustic response varies as a function of position along the length of the leaf.

B. Microscopic imagery

Examples of microscopic imagery of the seagrass leaf cross sections are shown in Fig. 5 for samples taken from the basal, middle, and apical sections of a seagrass leaf. While the width of the leaf remains approximately constant along its length, the basal end is 40% thicker than the middle and apical sections. Additionally, differences in the interior structure can also be observed, with significantly larger lacunae present in the basal cross section. Furthermore, the shape of the lacunae appears more circular in the middle and apical cross sections.

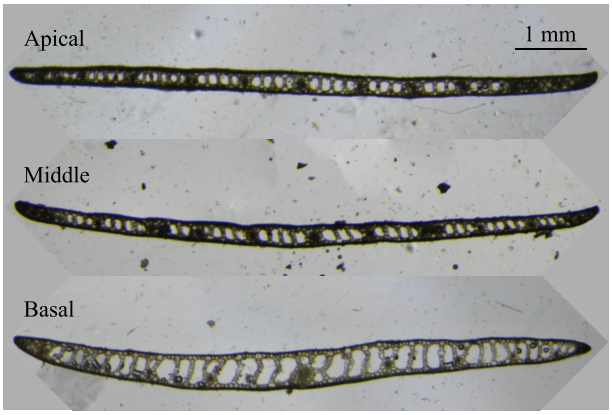

FIG. 5. (Color online) Microscopic imagery of cross sections taken from the apical, middle, and basal sections of a *T. testudinum* leaf.

Summary statistics for the basal, middle, and apical sections from ten seagrass leaves are shown in Fig. 6. The size of the lacunae is reported as the equivalent radius for a circle with the same area as the lacunae observed in the images. The basal section included the widest range of sizes and the largest lacunae, consistent with the imagery shown in Fig. 5. The distributions of lacuna sizes for the middle and apical sections were similar, but the middle section includes sizes with equivalent radii greater than 0.09 mm not observed in the apical section.

The void fraction, calculated as the area of leaf cross section occupied by lacunae relative to the total area, is shown in Fig. 6(b). Again, the basal section is the outlier, with a void fraction more than 50% greater than the middle and apical sections. The middle section has a slightly higher void fraction than the apical section, but the differences in the mean values do not exceed the variation between the sections as represented by the error bars. The greater void fraction observed in the basal section is consistent with the imagery shown in Fig. 5.

C. Torsional measurements

The shear modulus along the length of a seagrass leaf was determined by independently examining short sections of the leaf in the DMA. Each of the sections was cut to 3 cm in length and inserted into the DMA. Care was taken to keep the leaf moist, as leaves were noted to become more brittle

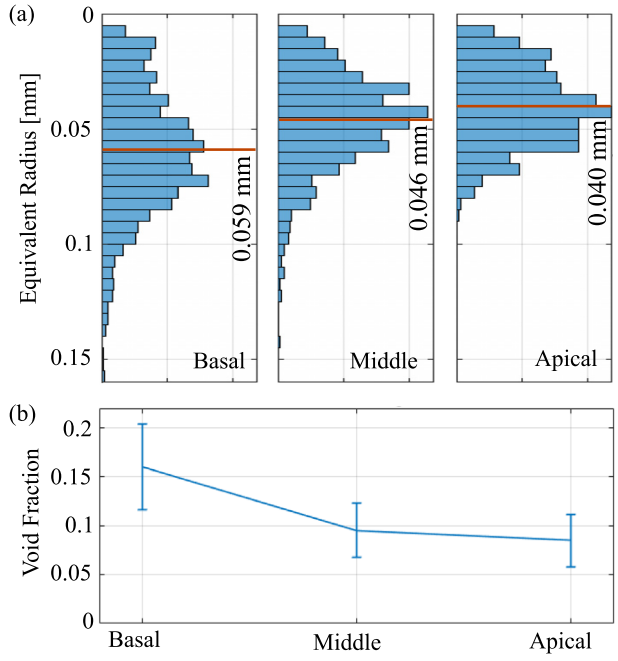

FIG. 6. (Color online) (a) Equivalent radii calculated for circular cross section with the same area as the lacunae from microscopic imagery of cross sections taken from the apical, middle, and basal sections of *T. testudinum* leaves. The orange line indicates the mean equivalent radii for each section. (b) Void fraction calculated as the volume ratio of lacunae to total leaf volume from microscopic imagery from the apical, middle, and basal sections of *T. testudinum* leaves. The error bars represent the standard deviation of measurements from different leaves.

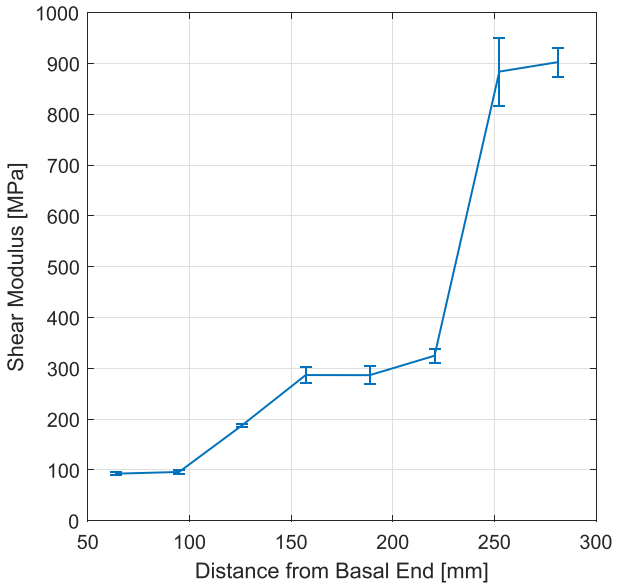

FIG. 7. (Color online) Shear modulus of a *T. testudinum* leaf measured by the DMA as a function of length along the leaf.

as they dry out. Figure 7 displays the low-frequency shear modulus averaged over the 0.3–1 Hz band. This band was chosen to omit some noisy data below 0.3 Hz and to avoid a slight increase in shear modulus at higher frequencies that may be associated with the leaf drying over the course of the measurement. The results show a trend of increasing shear modulus along the length of the leaf, with the measurements from the apical end having substantially greater values.

D. FEM model

1. Parameter sensitivity

A sensitivity study was performed to quantify the effects of model parameters on the effective sound speed of seagrass leaves in the resonator. The 2D simulations used leaf cross sections composed of an epidermis, aerenchyma, and lacunae. Leaf cross sections were created based on the microscopic imagery, although some simplifications were made for the FEM modeling. Lacunae with cross-sectional areas smaller than 2×10^{-4} mm^2 were eliminated, and the epidermis was set to a constant thickness. An example of a simplified leaf cross section used in the finite element modeling is shown in Fig. 8.

A set of default parameters was chosen based on previous measurements and modeling efforts. Then each parameter was perturbed, and the effective sound speed was calculated for the perturbed model and compared to that of the default model. The rest of this section describes the parameters, the choice of default value, and the effects of perturbing its value on the effective sound speed. The results are summarized in Table II. For all experiments, the volume fraction of gas and seagrass leaves within the resonator was fixed to values of 7.2×10^{-4} and 5.83×10^{-3} (gas also included), respectively.

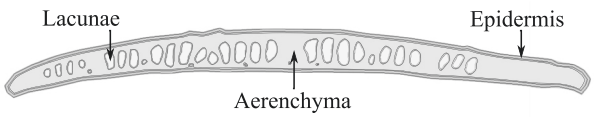

FIG. 8. One of the leaf cross sections used in the FEM modeling simulations.

The default value for epidermis thickness was estimated from the microscope image data. Analysis of these images revealed that thickness could vary between 0.02 and 0.07 mm with the average thickness being 0.035 mm. In creating the leaf model used in the FEM modeling, the thickness of the epidermis was set to a constant value. The default value was set to 0.03 mm, and perturbed thicknesses were approximately 30% larger and smaller. The simulation with the decreased/increased epidermis thickness resulted in an effective sound speed that was lower/higher than that of the default case, indicating the model was responsive to lower/higher resistance provided by the thinner/thicker epidermis. However, for both cases, the effective sound speed changed by less than 1%.

The default value of the leaf bulk modulus was determined in previous work. Enenstein *et al.* (2013) used a food blender to create a "seagrass soup" of finely divided *T. testudinum* leaf tissue suspended in seawater. Resonator measurements were performed on the mixture to determine an effective sound speed and calculate the bulk modulus. Since the mixture contained both tissue components, this value was applied to both the epidermis and aerenchyma in the FEM leaf model. The perturbations consider decreasing/increasing the default value by a factor of 2. Responsiveness of the simulation was shown by a decrease/increase in the effective sound speed for decrease/increase in the bulk modulus. However, for both cases, the effective sound speed changed by less than 1%.

The epidermis shear modulus was determined from the measurements presented in Sec. III C. The default value of

TABLE II. The change in the effective sound speed for perturbations to model parameters. The effective sound speed calculated using the default parameter values was 1174 m/s.

	Default parameter value	Perturbed parameter values	Effective sound speed (m/s)	Percent change (%)
Epidermis thickness (mm)	0.03	0.02	1167	0.6
		0.04	1183	0.8
Bulk modulus (MPa)	1.11	0.555	1168	0.5
		2.22	1178	0.3
Epidermis shear modulus (MPa)	400	200	1167	0.6
		800	1179	0.4
Aerenchyma shear modulus (MPa)	3.4	1.7	1013	13.7
		6.8	1306	11.2
Gas sound speed (m/s)	343	293	1169	0.4
		393	1178	0.3
Channel representation	Actual	Actual	1174	—
		Idealized	1162	1.0

https://doi.org/10.1121/10.0017000

400 MPa was chosen based on the results described in Sec. III C. The perturbations consider decreasing/increasing the default value by a factor of 2. Again, these simulations show the expected change in the effective sound speed, which is decreased/increased for smaller/larger values of the epidermis shear modulus. Nevertheless, the change to the effective sound speed is less than 1%.

The default value of 3.4 MPa for the aerenchyma shear modulus was chosen based on results from FEM modeling. The perturbations consider decreasing/increasing the default value by a factor of 2. These simulations show the resulting change in the effective sound speed, which is decreased/increased for smaller/larger values of the aerenchyma shear modulus. The change in the aerenchyma shear modulus had a significantly larger impact of the effective sound speed, shown by an effective sound speed change of over 10%.

In a previous study, Torres *et al.* (2020) determined that the accuracy of the FEM modeling simulations could be improved by accounting for the thermal properties of gas bubbles using an effective polytropic exponent to adjust the sound speed of the gas (Commander and Prosperetti, 1989; Miller, 1979). The chemical composition of the gas can also affect its sound speed. Analysis of gas ebullition in seagrass meadows suggests the oxygen content of the bubbles produced by photosynthesis is up to 20% greater than that of atmospheric air Long *et al.* (2020). To quantify the thermal effect as well as the chemical composition of the gas in the seagrass leaf channels on FEM simulations studied in this work, the gas sound speed was included as a parameter in the sensitivity study. The default value used the sound speed for air at ambient conditions 343 m/s, and the perturbed values were 343 ± 50 m/s. The simulations showed that overall, the effect of gas sound speed was small, with the change to the effective sound speed being less than 1%.

Two representations of the gas channels were considered: actual shapes based on the microscope imagery and idealized circular gas channels of equivalent area. The idealized shapes were considered because they were more computationally efficient to model and because the adjustment for the thermal effect was based on the assumption of cylindrical gas cavities. The use of idealized circular cross sections changed the effective sound speed by 1.0%. Since this value is more than 2 times greater than the perturbation to sound speed to account for thermal effects, it was deemed more important to accurately represent the lacuna shape than to account for the thermal gas properties.

2. Inference for aerenchyma shear modulus

As demonstrated by the parameter study, the shear modulus of the aerenchyma has the greatest effect on the effective sound speed of seagrass leaves and seawater in the acoustic resonator. The change in the effective sound speed caused by perturbing the aerenchyma shear modulus was more than an order of magnitude greater than the change caused by any other parameter. Furthermore, all other properties of the seagrass leaf model had been previously characterized by independent measurements. Therefore, using the measured effective sound speed from Sec. III A, a value for the aerenchyma shear modulus was inferred by fixing all other properties to the default values in Table II.

In the simulations, the volume fractions of gas and seagrass tissue were set to match that of the experiment as calculated from the microscopic imagery. To match the effective sound speed estimated from full-leaf measurements from Sec. III A 1, the FEM simulations used cross sections from along the length of the leaf. For comparison with the resonator measurements on leaf sections in Sec. III A 2, the simulations used leaf cross sections from the corresponding basal, middle, or apical section.

The results of the simulations are shown in Fig. 9. For each experiment, the simulations were performed for values of the aerenchyma shear modulus between 0.2 and 5 MPa, and a logarithmic fit to the calculated effective sound speed was calculated. The inferred shear modulus was taken as the point where the measured effective sound speed intersects the logarithmic fit. For this comparison, the measured effective sound speed was taken as the frequency average of the measurements shown in Figs. 3 and 4. The inferred values for the aerenchyma shear modulus are listed on Fig. 9. The fits have similar slopes, which is related to the shear modulus of the aerenchyma, and slight differences result from the various leaf geometries. The vertical shift in the fits is related to void fraction of gas present in the simulations. The lower/higher effective sound speed for the basal/apical sections was demonstrated in Sec. III A 2; the lower effective sound speed from the whole-leaf measurements results from the leaf volume fraction increased by including all of the sections.

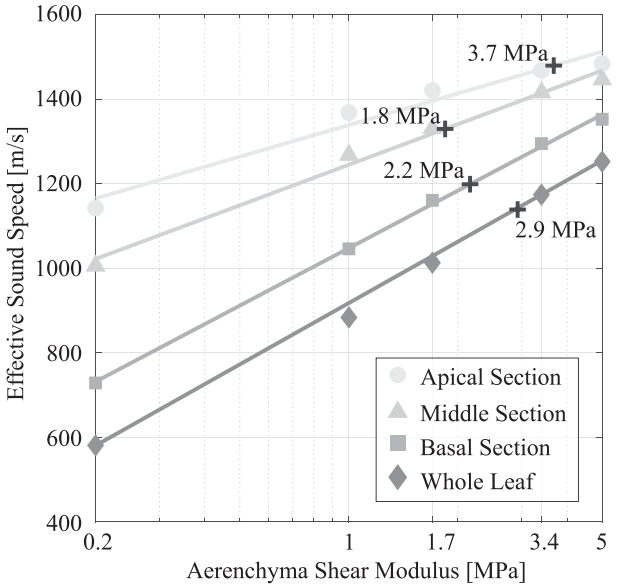

FIG. 9. Effective sound speed calculated by the FEM model and plotted as a function of aerenchyma shear modulus (gray symbols), logarithm fits to the simulation results (gray lines), and intersection of the fit with the measured effective sound speed (black crosses). The value of aerenchyma shear modulus that best fits the measured effective sound speed is listed on the plot.

IV. DISCUSSION

A. Aerenchyma shear modulus and comparison to previous measurements

Previous work determined that the elastic properties and the physical structure of seagrass leaves needed to be considered (Wilson *et al.*, 2010; Wilson and Dunton, 2009). This work established that the shear modulus of the aerenchyma was the most important parameter controlling the low-frequency effective-medium sound speed of seagrass leaves for a given void fraction. The addition of the epidermis is important for providing structure for the seagrass leaves, but it has a small effect on the effective sound speed as demonstrated by the results shown in Table II.

In comparing the results presented in Fig. 9 to preliminary results reported in Torres *et al.* (2020), the shear modulus inferred from the whole-leaf measurements was 40% higher. Although there were several differences in the FEM simulations, including the idealized lacuna shapes and lack of epidermis, the main difference in the inferred aerenchyma shear modulus is attributable to an inaccurate estimate of the void fraction of gas in the data presented in Wilson and Dunton (2009), which used one representative leaf cross section based on Phillips and Meñez (1988) that did not account for variability along the length of the leaf or leaf-to-leaf variability. The current paper uses high fidelity imagery of the leaves in the FEM model of the resonator. The accuracy of the aerenchyma shear modulus from the current work is supported by consistency between the leaf-section and whole-leaf measurements shown in Fig. 9 such that the aerenchyma shear modulus inferred from the whole-leaf measurements is approximately the mean of that of the leaf-section measurements.

B. Variability of properties along leaf length

The measurements presented in Sec. III revealed several characteristics of the variation in properties along the length of *T. testudinum* leaves. First, resonator measurements showed an approximately linear decrease in the effective sound speed of seagrass leaves moving from the apical section to the middle section to basal section. Next, an examination of the microscopic imagery of the seagrass showed the basal sections were characterized by significantly higher void fractions as well as larger lacunae. The observation of comparatively lower effective sound speed in the basal section is supported by the trend of higher void fraction of gas in this section. However, the difference in the effective sound speed between the middle and apical sections is not easily explained by the same argument as these sections display similar void fractions and lacuna sizes.

The DMA measurements shown in Fig. 7 highlighted a difference in the shear modulus of the apical section, which was significantly greater than that of the middle and basal sections. These data show the shear modulus of the leaf is approximately 3 times greater near the apical end of the leaf, which provides an explanation for the increased effective sound speed for this leaf section. The stiffer material at this end of the leaf restricts the acoustic response of the lacunae, and therefore there is a smaller effect on the effective sound speed.

The inferences from the FEM simulations are consistent with the DMA measurement as the results indicate a higher shear modulus in the aerenchyma in the apical section. As shown in Fig. 9, the shear modulus of the apical section is nearly twice that of the basal and middle sections. In making comparisons between Figs. 7 and 9, recall that the DMA measurements represent the shear modulus of the composite leaf section consisting of both the aerenchyma and the epidermis. However, the DMA measurements are most sensitive to the stiffer epidermis both because of its greater rigidity and its position on the outside of the leaf, which increases its polar moment of inertia. On the other hand, the FEM simulations were used to infer the shear modulus of the aerenchyma while holding a fixed value for the epidermis. This is because the acoustic response is most sensitive to the properties of the aerenchyma, which encapsulates the lacunae. Nevertheless, both the DMA measurements and the FEM simulations indicated the apical leaf section consists of more rigid tissue than the basal or middle section.

V. CONCLUSION

A new seagrass leaf model was developed for *T. testudinum* that consists of a stiffer epidermis and more compliant aerenchyma. The geometry of the leaf model was based on microscopic imagery taken from cross sections acquired from along the length of seagrass leaves. With the bulk modulus and density of the seagrass tissue determined by previous work, this study focused on characterizing the shear moduli of the epidermis and aerenchyma. Since the shear modulus of the aerenchyma was 2 orders of magnitude smaller than that of the epidermis, it did not significantly influence the torsional stress applied to the leaf. This difference in the rigidity of the two leaf components made it possible to independently characterize the shear modulus of the epidermis using torsional pendulum measurements and with the DMA. On the other hand, the lacunae were only in contact with the aerenchyma, and its shear modulus was established from low-frequency resonator measurements.

The complexity of the variability in properties along the length of the seagrass leaf was observed in the resonator measurements, DMA measurements, and microscopic imagery. These data indicated the basal ends of the *T. testudinum* leaves are more compliant, have larger lacunae, and have greater void fractions. On the other hand, apical ends are more rigid, with smaller lacunae and lower void fractions. Interestingly, these properties did not appear to have a linear gradient along the length of the leaf, with middle sections having similar lacunae and void fractions to the apical sections but having shear moduli more similar to the basal sections.

The new seagrass leaf model developed in this study, particularly seagrass tissue properties and their relative influence on acoustic propagation, will be used to inform

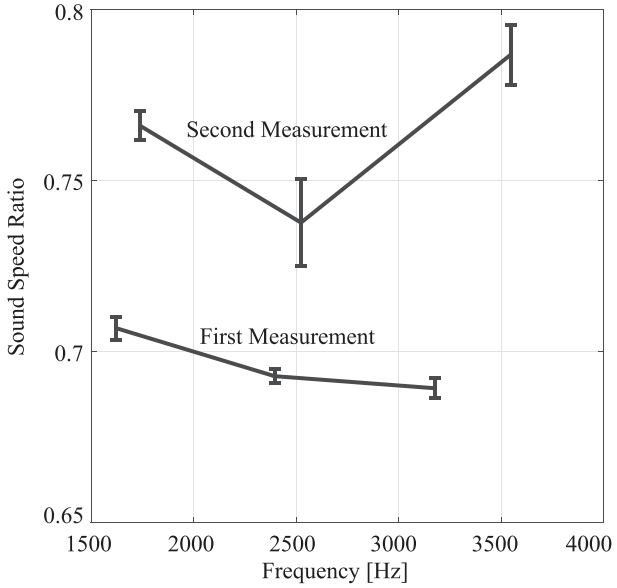

FIG. 10. Sound speed ratios calculated from a resonator experiment using degassed water. The first set of measurements was collected immediately after placing the seagrass in the resonator, and the second set of measurements was collected 3 h and 40 min later. Error bars represent the standard deviation of five sets of replicate measurements.

new mathematical models that account for the encapsulation of gas channels by the seagrass tissue as well as the shapes of lacunae. Such a model is needed to accurately predict acoustic propagation through seagrass to ultimately inform an inference for seagrass metabolic values, such as gross primary productivity and respiration (Ballard *et al.*, 2020).

ACKNOWLEDGMENTS

This work was supported by the ARL:UT Independent Research and Development Program, by the National Science Foundation under Award No. 2023211, and by the Office of Naval Research (ONR) Ocean Acoustics Program under Grant Nos. N00014-21-1-2245 and N00014-21-1-2254. The authors also thank Ken Dunton and Kyle Capistrant-Fossa for collection of seagrass samples and Nathan Wilson for assistance with the microscopic imagery.

APPENDIX

When seagrass was placed in degassed water, the gas from the lacunae diffused through the seagrass tissue into the surrounding seawater. This effect was observed experimentally as the effective sound speed calculated from seagrass leaves in the resonator increased over time. An example of this effect is displayed in Fig. 10, which shows the mean sound speed ratio changed by 0.07 over a time period of 3 h and 40 min.

Ballard, M., Lee, K. M., Capistrant-Fossa, K., McNeese, A. R., Sen, P., Jerome, T. S., Wilson, P. S., and Dunton, K. H. (**2022**). "A yearlong record of acoustic propagation and ambient sound in a seagrass meadow," J. Acoust. Soc. Am. **152**(4), A107.

Ballard, M. S., Lee, K. M., Sagers, J. D., Venegas, G. R., McNeese, A. R., Wilson, P. S., and Rahman, A. F. (**2020**). "Application of acoustical remote sensing techniques for ecosystem monitoring of a seagrass meadow," J. Acoust. Soc. Am. **147**(3), 2002–2019.

Bennett, D. L., Bister, T. J., and Ott, R. A., Jr. (**2020**). "Using recreation-grade side-scan sonar to produce classified maps of submerged aquatic vegetation," North Am. J. Fish. Manag. **40**(1), 145–153.

Chang, A. Y., Chiu, L. Y., Mok, M. H.-K., Soong, K., and Huang, W.-J. (**2019**). "Experimental observations of diurnal acoustic propagation effects in seagrass meadows on the Dongsha Atoll," J. Acoust. Soc. Am. **146**(3), EL279–EL285.

Church, C. C. (**1995**). "The effects of an elastic solid surface layer on the radial pulsations of gas bubbles," J. Acoust. Soc. Am. **97**(3), 1510–1521.

Commander, K. W., and Prosperetti, A. (**1989**). "Linear pressure waves in bubbly liquids: Comparison between theory and experiments," J. Acoust. Soc. Am. **85**(2), 732–746.

Del Grosso, V. (**1971**). "Analysis of multimode acoustic propagation in liquid cylinders with realistic boundary conditions–application to sound speed and absorption measurements," Acta Acust. united Acust. **24**(6), 299–311.

Dolder, C. N., and Wilson, P. S. (**2017**). "Using one-dimensional waveguide resonators to measure phase velocities in bubbly liquids," J. Acoust. Soc. Am. **141**(4), 2832–2839.

Enenstein, G., Dolder, C., Wilson, P. S., and Hermand, J.-P. (**2013**). "Investigation of low-frequency acoustic tissue properties of seagrass," Proc. Mtgs. Acoust. **19**(1), 005007.

Felisberto, P., Jesus, S. M., Zabel, F., Santos, R., Silva, J., Gobert, S., Beer, S., Björk, M., Mazzuca, S., Procaccini, G., Runcie, J. W., Champenois, W., and Borges, A. V. (**2015**). "Acoustic monitoring of O_2 production of a seagrass meadow," J. Exp. Mar. Biol. Ecol. **464**, 75–87.

Greene, A., Rahman, A. F., Kline, R., and Rahman, M. S. (**2018**). "Side scan sonar: A cost-efficient alternative method for measuring seagrass cover in shallow environments," Estuar. Coast. Shelf Sci. **207**, 250–258.

Gumusay, M. U., Bakirman, T., Kizilkaya, I. T., and Aykut, N. O. (**2019**). "A review of seagrass detection, mapping and monitoring applications using acoustic systems," Eur. J. Remote Sens. **52**, 1–29.

Hamana, M., and Komatsu, T. (**2016**). "Real-time classification of seagrass meadows on flat bottom with bathymetric data measured by a narrow multibeam sonar system," Remote Sens. **8**(2), 96.

Held, P., and Schneider von Deimling, J. (**2019**). "New feature classes for acoustic habitat mapping—A multibeam echosounder point cloud analysis for mapping submerged aquatic vegetation (SAV)," Geosciences **9**(5), 235.

Hermand, J.-P. (**2004**). "Photosynthesis of seagrasses observed *in situ* from acoustic measurements," in *Proceedings of Oceans' 04 MTS/IEEE Techno-Ocean'04 (IEEE Cat. No. 04CH37600)*, November 9–12, Kobe, Japan, Vol. 1, pp. 433–437.

Hermand, J.-P., Nascetti, P., and Cinelli, F. (**1998**). "Inversion of acoustic waveguide propagation features to measure oxygen synthesis by *Posidonia oceanica*," in *IEEE Oceanic Engineering Society. OCEANS'98. Conference Proceedings (Cat. No. 98CH36259)*, September 28–October 1, Nice, France, Vol. 2, pp. 919–926.

Hermand, J.-P., Nascetti, P., and Cinelli, F. (**2000**). "Inverse acoustical determination of photosynthetic oxygen productivity of *Posidonia* seagrass," in *Experimental Acoustic Inversion Methods for Exploration of the Shallow Water Environment* (Springer, Dordrecht, Netherlands), pp. 125–144.

Johnson, J. R. (**2019**). "Acoustic characterization of Mediterranean seagrasses *Posidonia oceanica* and *Cymodocea nodosa*," Ph.D. thesis, University of Texas at Austin, Austin, TX.

Kaldy, J. E., and Dunton, K. H. (**2000**). "Above- and below-ground production, biomass and reproductive ecology of *Thalassia testudinum* (turtle grass) in a subtropical coastal lagoon," Mar. Ecol. Prog. Ser. **193**, 271–283.

Klemens, K. W. (**2017**). "Development and evaluation of a USV based mapping system for remote sensing of eelgrass extent in Southern California," Ph.D. thesis, University of Southern California, Los Angeles, CA.

Kruss, A., Tgowski, J., Tatarek, A., Wiktor, J., and Blondel, P. (**2017**). "Spatial distribution of macroalgae along the shores of Kongsfjorden (West Spitsbergen) using acoustic imaging," Pol. Polar Res. **38**(2), 205–229.

Lafleur, L. D., and Shields, F. D. (**1995**). "Low-frequency propagation modes in a liquid-filled elastic tube waveguide," J. Acoust. Soc. Am. **97**(3), 1435–1445.
Lee, K. M., Ballard, M. S., McNeese, A. R., and Wilson, P. S. (**2017**). "Sound speed and attenuation measurements within a seagrass meadow from the water column into the seabed," J. Acoust. Soc. Am. **141**(4), EL402–EL406.
Lee, K. M., Ballard, M. S., McNeese, A. R., Wilson, P. S., Venegas, G. R., Zeh, M. C., and Rahman, A. F. (**2023**). "Inter-seasonal comparison of acoustic propagation in a *Thalassia testudinum* seagrass meadow in a shallow sub-tropical lagoon," JASA Express Lett. **3**, 010801.
Lee, K. M., Ballard, M. S., Venegas, G. R., Sagers, J. D., McNeese, A. R., Johnson, J. R., Wilson, P. S., and Rahman, A. F. (**2019**). "Broadband sound propagation in a seagrass meadow throughout a diurnal cycle," J. Acoust. Soc. Am. **146**(4), EL335–EL341.
Lee, K. M., Hinojosa, K. T., Wochner, M. S., Argo, T. F., Wilson, P. S., and Mercier, R. S. (**2011**). "Sound propagation in water containing large tethered spherical encapsulated gas bubbles with resonance frequencies in the 50 Hz to 100 Hz range," J. Acoust. Soc. Am. **130**(5), 3325–3332.
Lee, K.-S., and Dunton, K. H. (**1996**). "Production and carbon reserve dynamics of the seagrass *Thalassia testudinum* in Corpus Christi Bay, Texas, USA," Mar. Ecol. Prog. Ser. **143**, 201–210.
Lenhart, R. D., Sagers, J. D., and Wilson, P. S. (**2016**). "Development of a standing wave apparatus for calibrating acoustic vector sensors and hydrophones," J. Acoust. Soc. Am. **139**(1), 176–187.
Long, M. H., Sutherland, K., Wankel, S. D., Burdige, D. J., and Zimmerman, R. C. (**2020**). "Ebullition of oxygen from seagrasses under supersaturated conditions," Limnol. Oceanogr. **65**(2), 314–324.
Mallock, A. (**1910**). "The damping of sound by frothy liquids," Proc. R. Soc. London, Ser. A **84**(572), 391–395.
Miller, D. L. (**1979**). "A cylindrical-bubble model for the response of plant-tissue gas bodies to ultrasound," J. Acoust. Soc. Am. **65**(5), 1313–1321.
Orth, R. J., Carruthers, T. J., Dennison, W. C., Duarte, C. M., Fourqurean, J. W., Heck, K. L., Hughes, A. R., Kendrick, G. A., Kenworthy, W. J., Olyarnik, S., Short, F. T., Waycott, M., and Williams, S. L. (**2006**). "A global crisis for seagrass ecosystems," Bioscience **56**(12), 987–996.
Pasqualini, V., Pergent-Martini, C., and Pergent, G. (**1999**). "Environmental impact identification along the Corsican coast (Mediterranean Sea) using image processing," Aquat. Bot. **65**(1), 311–320.
Pergent, G., Monnier, B., Clabaut, P., Gascon, G., Pergent-Martini, C., and Valette-Sansevin, A. (**2017**). "Innovative method for optimizing side-scan sonar mapping: The blind band unveiled," Estuar. Coast. Shelf Sci. **194**, 77– 83.
Phillips, R. C., and Meñez, E. G. (**1988**). *Seagrasses* (Smithsonian Institution, Washington, DC).
Rahnemoonfar, M., and Dobbs, D. (**2019**). "Semantic segmentation of underwater sonar imagery with deep learning," in *Proceedings of IGARSS 2019-2019 IEEE International Geoscience and Remote Sensing Symposium*, July 28–August 2, Yokohama, Japan, pp. 9455–9458.
Short, F., Carruthers, T., Dennison, W., and Waycott, M. (**2007**). "Global seagrass distribution and diversity: A bioregional model," J. Exp. Mar. Biol. Ecol. **350**(1), 3–20.
Stocks, J. R., Rodgers, M. P., Pera, J. B., and Gilligan, D. M. (**2019**). "Monitoring aquatic plants: An evaluation of hydroacoustic, on-site digitising and airborne remote sensing techniques," Knowl. Manag. Aquat. Ecosyst. **420**, 27.
Torres, N. A. (**2022**). "Modeling the low-frequency response of seagrass in a resonator tube," Master's thesis, University of Texas at Austin, Austin, TX.
Torres, N. A., Ballard, M. S., Lee, K. M., Venegas, G. R., and Wilson, P. S. (**2020**). "Inferring elastic properties of seagrass tissue from its acoustic response using finite element analysis," Proc. Mtgs. Acoust. **42**, 005001.
van Rein, H., Brown, C., Quinn, R., Breen, J., and Schoeman, D. (**2011**). "An evaluation of acoustic seabed classification techniques for marine biotope monitoring over broad-scales (>1 km^2) and meso-scales (10 m^2–1 km^2," Estuar. Coast. Shelf Sci. **93**(4), 336–349.
Venegas, G. R., Congdon, V. M., Torres, N. A., Ballard, M. S., Lee, K. M., Dunton, K. H., and Wilson, P. S. (**2020**). "Measuring the complex shear modulus of seagrass with an iPhone: A COVID–19 experiment (A)," J. Acoust. Soc. Am. **148**, 2748.
Waycott, M., Duarte, C. M., Carruthers, T. J., Orth, R. J., Dennison, W. C., Olyarnik, S., Calladine, A., Fourqurean, J. W., Heck, K. L., Hughes, A. R., Kendrick, G. A., Kenworthy, W. J., Short, F. T., and Williams, S. L. (**2009**). "Accelerating loss of seagrasses across the globe threatens coastal ecosystems," Proc. Natl. Acad. Sci. U.S.A. **106**(30), 12377–12381.
Wilson, C. J., Wilson, P. S., Greene, C. A., and Dunton, K. H. (**2010**). "Seagrass leaves in 3-D: Using computed tomography and low-frequency acoustics to investigate the material properties of seagrass tissue," J. Exp. Mar. Biol. Ecol. **395**(1-2), 128–134.
Wilson, P. S., and Dunton, K. H. (**2009**). "Laboratory investigation of the acoustic response of seagrass tissue in the frequency band 0.5–2.5 kHz," J. Acoust. Soc. Am. **125**(4), 1951–1959.
Wilson, P. S., Reed, A. H., Wilbur, J. C., and Roy, R. A. (**2007**). "Evidence of dispersion in an artificial water-saturated sand sediment," J. Acoust. Soc. Am. **121**(2), 824–832.
Wilson, P. S., and Roy, R. A. (**2008**). "An audible demonstration of the speed of sound in bubbly liquids," Am. J. Phys. **76**(10), 975–981.
Wood, A. B. (**1946**). *Textbook of Sound* (Bell, London).